

Avalanche Dynamics and the Effect of Straining in Dislocation Systems with Quenched Disorder

Dénes Berta, Barna Mendei, and Péter Dusán Ispánovity
*Eötvös Loránd university, Department of Materials Physics,
 Pázmány Péter sétány 1/A, 1117 Budapest, Hungary*

The plastic deformation of crystalline and other heterogeneous materials often manifests in stochastic intermittent events indicating the criticality of plastic behavior. Previous studies demonstrated that the presence of short-ranged quenched disorder modifies this behavior disrupting long-range static and dynamic correlations consequently localizing dislocation avalanches. However, these observations were mostly confined to relaxed materials devoid of deformation history. In this work our focus is on how straining affects static and dynamic correlations, avalanche dynamics and local yield stresses. We demonstrate that the interplay between severe straining and confining quenched disorder induces critical behavior characterized by dislocation avalanches distinct from those at lower stresses. Namely, near the flow stress many avalanches, even if triggered locally, evolve into events affecting a larger region by exciting small clusters of dislocations all around the sample. This type of avalanches differ from the ones at low strains where plastic events typically consist of one compact cluster of dislocations which is either local or it is already quite extended at the onset of the avalanche. Furthermore, we examine the impact of avalanches on local yield stresses. It is shown in detail in this work that while some statistical features of the local yield thresholds are robust to straining, others are significantly affected by the deformation history.

I. INTRODUCTION

Previous experimental results revealed that the plastic behavior of micron and sub-micron scale crystalline specimens fundamentally differ from that of their bulk counterparts. In this regime size-related hardening is observable [1–3], the deformation manifests as stochastic sequence of strain bursts [4, 5] that are often also accompanied by acoustic emission [6–9]. This stochasticity results in unpredictable plasticity and a zig-zag pattern in the stress-strain curves in contrast with the smooth behavior of bulk samples. In crystalline materials these fluctuations are results of sudden rearrangements of dislocations known as dislocation avalanches. Similar behavior characterizes other heterogeneous materials such as amorphous materials or foams in which the fluctuations are related to shear transformation zones [10, 11] and T1 events [12–14], respectively.

Despite the stochastic and seemingly unpredictable nature of plasticity of heterogeneous materials, several attempts have been made to establish a direct connection between the features of the microstructure and the emergent plastic response [15]. One of the most powerful predictor of the plastic behavior is the so-called *local yield stress*, that is, the critical stress at which the material yields during local probing. This descriptor was first showed to be a powerful tool of predicting the loci of plastic events in model amorphous solids [16] and then its applicability was demonstrated in crystalline materials modeled by discrete dislocation systems as well [17]. Numerical studies on metallic glasses revealed that the statistics of local yield stresses strongly depend on the preparation protocol [18]. In the case of crystalline materials it was shown that global plasticity is related to the local yield stresses through the weakest-link principle, however, this weakest-link picture is fundamentally

different depending on whether long- or short-range interactions dominate the dislocation dynamics [17]. Namely, in systems dominated by long-range elastic dislocation-dislocation interactions plastic events are spatially extended which leads to a weakest-link behavior of moderate consistency. If, however, a significant extent of short-ranged quenched disorder (e.g., point defects) is introduced, the plastic events get localized and a more rigorous traditional weakest-link picture is realized. This is related to the concept of the *wild to mild* transition which explains the empirical observation that depending on the interaction involved a material may exhibit very intense or very mitigated acoustic emission fluctuations during deformation [8].

As it was discussed above, the local yield stress is a very important indicator of the plasticity of materials and it connects the plastic behavior with structural properties through the weakest-link principle. This makes local yield stresses very important ingredients of mesoscale models because they can be utilized to introduce local strength fluctuations characteristic to heterogeneous materials [19, 20]. While it was shown for amorphous solids that the local yield thresholds correlate with plastic activity even after several plastic rearrangements it is still unknown how local yield stresses evolve if materials are exposed to significant deformation. Its importance from the mesoscopic modeling point of view comes from the need to understand how the local strengths have to be updated as the system evolves and deformation occurs and how their statistics is influenced by the deformation history. In this work we investigate these questions as well as the effect of deformation history in the framework of 2D discrete dislocation dynamics (DDD). One of the other foci of this work is how static (structural) and dynamic correlations and avalanche dynamics are affected by straining (nearly up to the phase transition to

sustained plastic flow) as well as by subsequent unloading of the sample.

The paper is structured as follows. After a summary of the model applied, the static correlations are investigated, then the focus is moved to the dynamic correlations. This is followed by an analysis of the plastic events carried out on the level of individual dislocations, and three distinct regimes of avalanche behavior are identified. Finally, local yield stresses are studied and the paper is concluded with a discussion and an outlook.

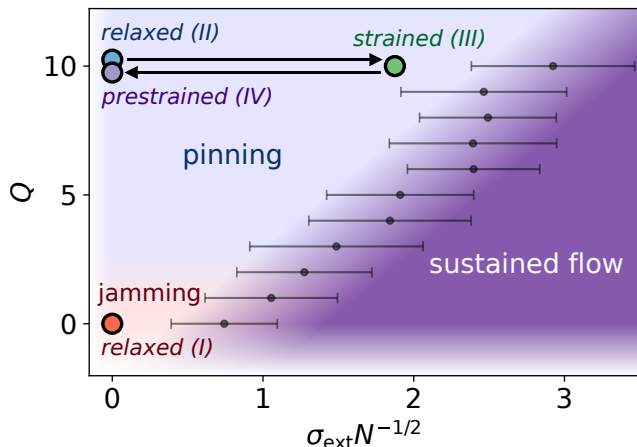


FIG. 1. The phase diagram of 2D discrete dislocation systems with quenched disorder. σ_{ext} and N are the external stress and the number of dislocations, respectively. Q is the ratio of the number of point defects and dislocations characterizing the extent of quenched disorder in the system. The markers indicate the four scenarios that are investigated in this paper. The relaxed $Q = 0$ system (scenario I) is governed by long-range dislocation-dislocation interactions and the case of dislocation jamming is realized. The $Q = 10$ systems are dominated by the short-range point defect - dislocation interactions, that is, it lies in the pinning regime. Besides the relaxed $Q = 10$ configurations (scenario II) two other types of $Q = 10$ systems were studied. The configurations were first strained close to the phase transition to sustained flow (scenario III). Then, the configurations are unloaded to zero external stress (scenario IV). The errorbars indicate the normalized stress at which the configuration enters the state of sustained plastic flow.

II. SIMULATION METHODS

In order to study the issues outlined in the introduction a 2D discrete dislocation dynamics (DDD) model is applied. This model, despite its simplicity, has proven to capture the main features of the criticality of crystalline plasticity since it was shown to be statistically consistent with experiments in terms of strain burst distribution, time distribution of dislocation avalanches, etc. [5, 9]. Additionally, the relatively simple setup (to be discussed in the next paragraph) allows us to study the

large-strain regime (even close to the phase of sustained plastic flow) which is immensely more challenging with more complex 3D DDD models or lower scale molecular dynamics (MD) approaches that are typically limited to small strains and/or system sizes.

In the model a square-shaped ($L \times L$ sized) simulation cell is considered that contains $N = 1024$ edge dislocations with line directions perpendicular to the xy plane of the simulation cell. Half of the dislocations have a Burgers vector of $\mathbf{b} = b\mathbf{e}_x$ and the other half have $\mathbf{b} = -b\mathbf{e}_x$ where b is the magnitude of the Burgers vectors and \mathbf{e}_x is the unit vector in direction x . The motion of the dislocations is restricted to slip motion in the direction x and they interact via a shear stress field of

$$\tau_d(\mathbf{r}) = \frac{\mu b}{2\pi(1-\nu)} \frac{x(x^2 - y^2)}{(x^2 + y^2)^2} \quad (1)$$

where $\mathbf{r} = (x, y)$ is the relative position with respect to a dislocation and μ and ν are the shear modulus and the Poisson's ratio, respectively. We note that in the paper stresses are normalized by stress units $\tau_0 = \frac{\mu b \sqrt{\rho}}{2\pi(1-\nu)}$ where $\rho = N/L^2$ is the dislocation density. Besides dislocations, the configurations may contain point defects introducing short-ranged quenched disorder to the system. The point defects are immobile but they interact with the dislocations via their shear stress fields of

$$\tau_v(\mathbf{r}) = -2Axy \frac{\frac{1 - \exp[-K^2 r^2]}{r^2} - K^2 \exp[-K^2 r^2]}{r^2} \quad (2)$$

where $\mathbf{r} = (x, y)$ is the relative position with respect to the point defect, A and K are constants characterizing the strength and the range of the stress field of the point defect. Based on Ref. [21] these parameters were chosen as $A = 0.0016 \tau_0 L^2 / \sqrt{N}$ and $K = 103.125 \sqrt{N}/L$. The extent of quenched disorder is quantified by the ratio $Q = N_p/N$ of the number of point defects N_p and the number of dislocations N . In our simulations Q is either 0 (no point defects) or 10 (10240 point defects in each configuration). While several novel methods have been developed to handle boundary conditions [22–24], surface effects are outside of the scope of this work, therefore, periodic boundary conditions (PBC) are applied for simplicity. PBC was implemented according to the procedure described in Ref. [25]. The dynamics of dislocations is governed by the dislocation-dislocation interactions, point defect - dislocation interactions and potentially homogeneous external stress acting on the dislocations. The emerging stiff system of differential equations is solved with an efficient implicit numerical scheme described in detail in Ref. [25] that provides a solution with practically no error beyond numerical precision.

The configurations are prepared in the following way. The dislocations (and point defects) are positioned randomly according to a 2D uniform distribution. Then, the configuration is let to relax and find a metastable configuration while no external stress is applied. This

relaxation may be followed by subsequent loading as described later. In our work we studied the ensembles of 100 configurations of each type (see examples of relaxed configurations in Fig. 2). The states at which the behavior of the configurations are investigated are summarized in Fig. 1. In total four different scenarios are studied (which are referred to as scenario I, II, III and IV later in the paper).

- (I) Configurations without point defects ($Q = 0$) relaxed at zero external stress.
- (II) Configurations with point defects ($Q = 10$) relaxed at zero external stress.
- (III) Configurations with point defects ($Q = 10$) that are strained close to the state of sustained plastic flow by applying a spatially homogeneous external stress $\sigma_{\text{ext}} = 1.875\tau_0\sqrt{N}$. The strained state is achieved by instantaneously increasing the external stress from zero to the desired value and then letting the system to find a new equilibrium state.
- (IV) Prestrained configurations with point defects ($Q = 10$) that are obtained from scenario III by instantaneously unloading the systems (that is, decreasing the external stress to zero) and letting them to relax. These configurations only differ from scenario II in their prestraining history.

The dynamical behavior and local yield stresses of these four scenarios listed above were studied by examining the avalanches triggered by quasi-static loading with a spatially homogeneous external stress. An avalanche is considered to have started when the mean dislocation velocity exceeds a predefined threshold $v_{\text{thr}} = 10^{-4}v_0$. $v_0 = \frac{\mu b^2 \sqrt{\rho}}{2\pi(1-\nu)B}$ is the unit of velocities in our simulations where μ is the shear modulus, b is the length of the Burgers vector, ρ is the dislocation density, ν is the Poisson ratio and B the dislocation drag coefficient characterizing dislocation mobility. When the mean velocity drops again below this threshold, the avalanches are considered to have ceased (see Fig. 5). For more details of the loading and avalanche detection protocol during local yield stress measurements see the corresponding section on local yield stresses and Ref. [23].

III. RESULTS

A. Static correlations

The static correlations of the dislocation configurations are studied by computing the two-point correlation function

$$d_s(\Delta\mathbf{r}) = \frac{\rho_s^{(2)}(\Delta\mathbf{r})}{\langle \rho_s^{(2)} \rangle} - 1 \quad (3)$$

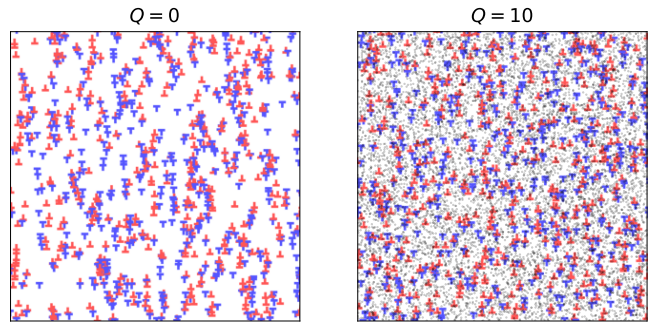


FIG. 2. Two representative configurations of relaxed discrete dislocation systems for cases $Q = 0$ and $Q = 10$ where Q is the ratio of the number of point defects and dislocations. ‘T’ shaped markers indicate the positions of edge dislocations red and blue ones corresponding to dislocations with Burgers vectors pointing to the positive and the negative x direction, respectively. The small gray markers denote the position of the point defects.

where $\Delta\mathbf{r}$ is the relative position of two dislocations of the same sign and $\rho_s^{(2)}$ is the two-point density of same-signed dislocations. $d > 0$ means that the relative position is more frequent than in a completely random configuration and $d < 0$ corresponds to a relative position which is less likely. The correlation maps are shown in Fig. 3. It is obvious that horizontally and especially vertically there is a strong correlation of dislocations (that is, a dislocation favors a position below or above another one of the same sign). We note that the correlation of opposite-signed dislocations was previously shown to be shorter-range [26], therefore, we only focus on the same-signed correlations in this work. In order to characterize the range of static correlations, the spatial dependence of the correlation function was computed in the vertical direction within a narrow cone of central angle of $\varphi = 2 \cdot \tan^{-1}(1/10) \approx 11.4^\circ$. The correlation functions in the vertical direction obeys

$$d_s(\Delta r) \propto (\Delta r)^{-\alpha} \exp \left[-\frac{\Delta r}{\xi_s} \right] \quad (4)$$

where $\alpha \approx 1.5$ (as derived in Ref. [27] using a variational approach) for all four distinct scenarios investigated but the static correlation length ξ_s is affected by the extent Q of quenched disorder and the straining history (see Fig. 4). The correlations are the strongest $Q = 0$ systems (scenario I) and the data suggests data the $d_s(\Delta r)$ has no cutoff or the cutoff length is large ($\xi_s \gtrsim L$). However, long-range correlations are disrupted by the quenched disorder leading to a static correlation length of $\xi \approx L/4$ in scenario II. One could expect that these correlations get stronger and the static correlation length diverges during straining as the system approaches the phase-transition to the sustained flow state. The prefactor of the dislocation-dislocation correlation, however, gets smaller as the system gets severely strained (scenario III) and it remains small as the system is unloaded

(scenario IV). Meanwhile, the correlation length indeed seems to diverge due to the straining with no apparent exponential cutoff in d_s in scenarios III and IV.

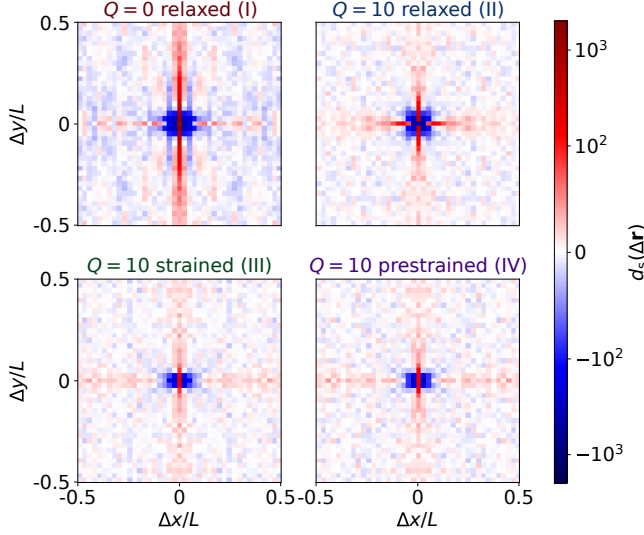


FIG. 3. The two-point correlation d_s of same-signed dislocations (for the definition see Eq. (3)). In the horizontal and vertical directions (in the latter, in particular) the dislocation configurations are strongly correlated especially in systems without quenched disorder ($Q = 0$).

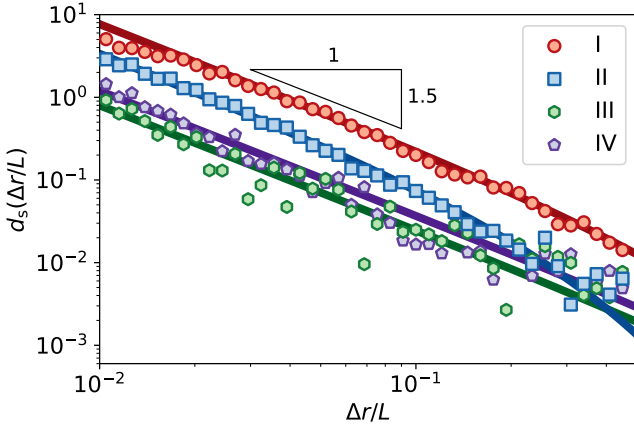


FIG. 4. The two-point correlation d_s of same-signed dislocations in the vertical direction (for the definition see Eq. (3)). $\Delta r/L$ is the distance of dislocations normalized with the simulation box size. The correlation decays with an exponent of 1.5. In scenario II the correlation has an exponential cutoff characterized by the static correlation length $\xi_s \approx L/4$. In the other three scenarios the data suggest that either there is no cutoff or it is much larger ($\xi_s \gtrsim L$).

B. Dynamic correlations

In the previous section the static (configurational) correlations were studied. In this section we address the issue whether and how the deformation state and deformation history affects the dynamics of the system. To this end we define the two-point velocity correlation $\langle v_i v_j \rangle$ as,

$$\langle v_i v_j \rangle(\Delta \mathbf{r}) = \left\langle \sum_{i=1}^{N_d} \sum_{\substack{j=1, \\ j \neq i}}^{N_d} \delta_D(\Delta \mathbf{r} - \mathbf{r}_i + \mathbf{r}_j) v_i v_j \right\rangle \quad (5)$$

where N_d , \mathbf{r} and v are the number of dislocations, their position vector and magnitude of velocity, respectively. δ_D denotes the Dirac delta generalized function. In a similar fashion the two-point displacement correlation $\langle \Delta x_i \Delta x_j \rangle$ is defined as

$$\langle \Delta x_i \Delta x_j \rangle(\Delta \mathbf{r}) = \left\langle \sum_{i=1}^{N_d} \sum_{\substack{j=1, \\ j \neq i}}^{N_d} \delta_D(\Delta \mathbf{r} - \mathbf{r}_i + \mathbf{r}_j) \Delta x_i \Delta x_j \right\rangle \quad (6)$$

where Δx is the displacement of an individual dislocation.

$\langle v_i v_j \rangle$ is computed for instantaneous velocities of individual dislocations and $\langle \Delta x_i \Delta x_j \rangle$ is evaluated for their displacements during given time intervals. Dislocation positions are evaluated at the moment at which the instantaneous velocities are considered or at the beginning of the studied interval in the case of displacement correlations. In the following $\langle v_i v_j \rangle$ is evaluated at the triggering of the first avalanche (that is when the mean dislocation velocity exceeds the predefined threshold v_{thr}) and $\langle \Delta x_i \Delta x_j \rangle$ is evaluated during the avalanche (i.e., for the interval starting at the triggering and ending when the mean dislocation velocity drops below v_{thr} , see Fig. 5). In this section the long-range asymptotic behavior of $\langle v_i v_j \rangle$ and $\langle \Delta x_i \Delta x_j \rangle$ is under inspection. We note that the instantaneous velocity and displacement correlations can be also interpreted as correlations of plastic strain rate and correlations of accumulated plastic strain contributions of individual dislocations, respectively.

At the onset of the first avalanche (during triggering) the asymptotic behavior is

$$\langle v_i v_j \rangle(\Delta \mathbf{r}) \propto \Delta r^{-\delta_{\text{trg}}} \quad (7)$$

where $\Delta r = |\Delta \mathbf{r}|$ is the distance of two dislocations. Figure 6 shows that in the critical $Q = 0$ case (scenario I) the triggered dislocation clusters are very extended already upon the onset of the avalanche with a low value of $\delta_{\text{trg}} \approx 1.0$ (see inset). In the presence of point defects (scenario II), however, the decay of $\langle v_i v_j \rangle$ is much faster with $\delta_{\text{trg}} \approx 1.8$. Perhaps contra-intuitively during straining (scenario III) and approaching the phase of sustained flow the triggered cores are not getting more extended, on the contrary, they are even more localized with $\delta_{\text{trg}} \approx 2.1$. After unloading (scenario IV) the system

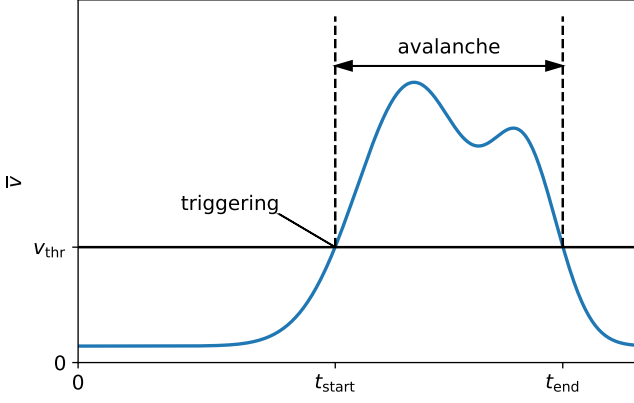


FIG. 5. The schematic illustration of how the correlations $\langle v_i v_j \rangle$ or $\langle \Delta x_i \Delta x_j \rangle$ are evaluated. $\langle v_i v_j \rangle$ is computed at time t_{start} , that is, at the onset of the avalanche, when the mean dislocation velocity \bar{v} exceeds a predefined threshold v_{thr} . $\langle \Delta x_i \Delta x_j \rangle$ is computed for the duration of the avalanche. This is the time interval starting at t_{start} and ending at time t_{end} when \bar{v} drops below v_{thr} .

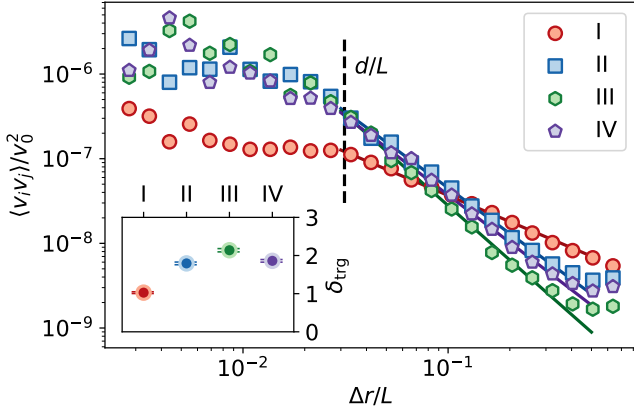


FIG. 6. The velocity correlation $\langle v_i v_j \rangle$ normalized with v_0^2 at the triggering of the first avalanche. For the definition of v_0 see the main text. The inset shows the exponents δ_{trg} defined in Eq. 7. The dashed line indicates d/L which denotes the average dislocation spacing normalized with the linear box size L .

again has the $\langle v_i v_j \rangle$ behavior seen in the relaxed $Q = 10$ state.

The displacement correlation $\langle \Delta x_i \Delta x_j \rangle$ is computed based on the displacements during the first avalanche. It also exhibits an asymptotic powerlaw dependence on Δr with an exponent δ_{ava} . That is, the asymptotic behavior reads as

$$\langle \Delta x_i \Delta x_j \rangle(\Delta \mathbf{r}) \propto \Delta r^{-\delta_{\text{ava}}}. \quad (8)$$

As it clear from Fig. 7 the picture that emerges about the spatial extension of avalanches only partly matches the one seen for the activation cores. Similarly to the case of triggered cores, the avalanches are also quite extended in dislocation systems without quenched disorder

(scenario I) characterized by an exponent $\delta_{\text{ava}} \approx 0.5$. A significantly higher value of exponent of $\delta_{\text{ava}} \approx 1.4$ at the relaxed $Q = 10$ case (scenario II) indicates that the introduction of point defects localizes not only the activation cores but the emerging dislocation avalanches as well. This exponent remains high (in fact, even grows) in the prestrained configuration (scenario IV) as well. However, for severely strained systems (scenario III) $\delta_{\text{ava}} \approx 0.7$ shows that as the system approaches the transition to sustained plastic flow, it starts to behave similarly to the critical $Q = 0$ case (scenario I) in terms of the spatial extension of the avalanches.

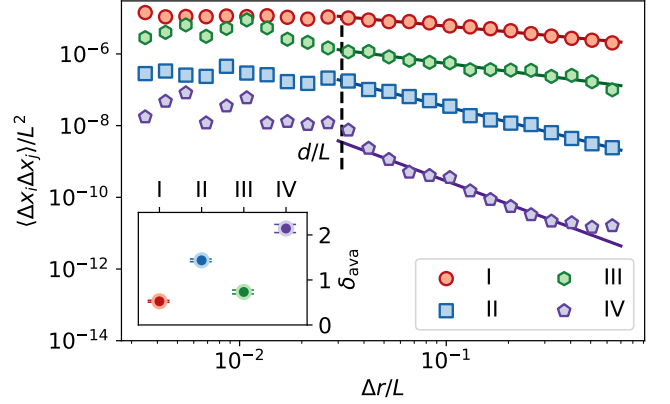


FIG. 7. The displacement correlation $\langle \Delta x_i \Delta x_j \rangle$ for displacements of individual dislocations during the first avalanche. The inset show the exponents δ_{tot} defined in Eq. 8. The dashed line indicates d/L which denotes the average dislocation spacing normalized with the linear box size L .

In this paragraph the tendencies in the dynamical correlations are summarized. The exponents δ of scenario I and II are quite consistent. In the former case the exponents are low ($0 < \delta < 1$) indicating that the dynamically affected regions of the system are quite extended in space. In the latter case the exponent are significantly higher (around 0.8 – 0.9 higher in each case) corresponding to a much more localized dynamic behavior. The strained (loaded) $Q = 10$ systems (scenario III), however, exhibit a more complex dynamic pattern. Activation cores (where the triggering of the avalanche happens) are still localized (surprisingly even more than in the relaxed systems) but the dynamical correlations in whole avalanches is much longer-ranged (such as in scenario I). This is consistent with what one would expect being close to the phase transition to sustained flow since correlations lengths near phase transition tend to diverge (e.g. near the Curie point in the context of magnetization). The prestrained systems (scenario IV) have similar dynamical correlations to its relaxed counterpart without any straining history (scenario II), in fact, our simulations show that their behavior at the onset of the first avalanche is practically indistinguishable based on distance dependence of $\langle v_i v_j \rangle$. We note that both for the triggering and for the whole avalanches the pow-

erlaw regime quantified by the exponent δ was prevalent over the normalized characteristic dislocation spacing $d/L = 1/\sqrt{\rho}L = 1/\sqrt{N}$. Below d/L typically we obtained roughly constant (distance-independent) velocity and displacement correlations. This indicates that the dislocations that contribute the most to these correlations (i.e. the ones at the very core of the avalanche) typically have comparable velocities irrespective of their actual distance.

C. Participation number

In the previous section the spatial range of dynamic correlations was examined. In the following the number of dislocations involved in the (first) avalanches is studied by introducing the participation number (PN). PN characterizes the number of moving dislocations [28] and is defined as

$$\text{PN}(v) = \frac{\left(\sum_{i=1}^N |v_i|^2\right)^2}{\sum_{i=1}^N |v_i|^4}. \quad (9)$$

Analogously, if the aim is to quantify the dynamic behavior integrated for a time interval instead of an instantaneous dynamic state, the displacement-based version of the participation number can be defined as

$$\text{PN}(\Delta x) = \frac{\left(\sum_{i=1}^N |\Delta x_i|^2\right)^2}{\sum_{i=1}^N |\Delta x_i|^4}. \quad (10)$$

Here v_i and Δx_i are the velocity and the displacement of the i th dislocation, respectively. In the special case of N' dislocations moving with the same velocity and $N - N'$ dislocations being still PN simply takes on the value of N' . In a general case (potentially all dislocation velocities being different) PN is typically non-integer but stays within the bounds of 1 and N and characterizes the number of dislocations having significant velocities/displacements (compared to the other ones).

The probability density functions P of $\text{PN}(v)$ and $\text{PN}(\Delta x)$ are shown in Fig. 8. The results clearly show that more dislocations are involved in both the triggering and the whole avalanche in the $Q = 0$ systems (scenario I) than in the $Q = 10$ ones (scenarios II, III and IV) irrespective of the deformation history. It can be observed that different straining history does not yield a striking difference between the average behavior of $Q = 10$ systems in terms of the participation number (neither at triggering nor for the whole avalanches). It is somewhat contradictory with the more pronounced differences that were shown in the case of dynamic correlations. In the following section the structure of the avalanches is studied (on the level of individual dislocations) and it is demonstrated that strained configurations (with short-range quenched disorder) can produce avalanches that are spatially quite extended despite having a relatively

small number of dislocations involved (which resolves the above mentioned seeming contradiction).

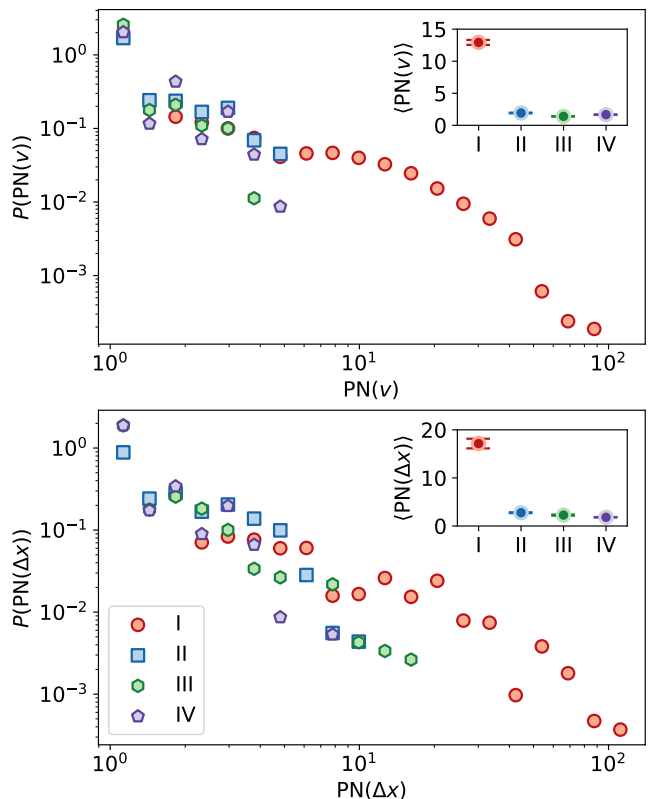


FIG. 8. The probability density function P of the participation number PN based on velocities ($\text{PN}(v)$) or displacements ($\text{PN}(\Delta x)$). For the definition see Eqs. (9) and (10). (Top): The PN based on the instantaneous velocities at the onset of the first avalanche. (Bottom): The PN based on the accumulated displacements during the first avalanche. The insets show the mean PN values and their uncertainty estimated with the Jackknife method.

D. Avalanche structure

As it was mentioned previously, when comparing the data in terms of participation numbers and spatial dynamic correlations, the results might seem somewhat contradictory in the case of strained $Q = 10$ systems (scenario III). Namely, while during the avalanches the asymptotic $\langle \Delta x_i \Delta x_j \rangle$ behavior of these systems tends towards the same exponent as for the critical $Q = 0$ configurations (scenario I), in terms of PN the strained systems are still much closer to the relaxed $Q = 10$ case (scenario II) which contains much more localized events than scenario I. That is, while the avalanches in strained configurations show longer-range dynamical correlations the number of dislocations involved certainly do not seem to grow proportionally. In order to address this discrepancy, in the following the plastic events are analyzed on

the level of individual dislocations.

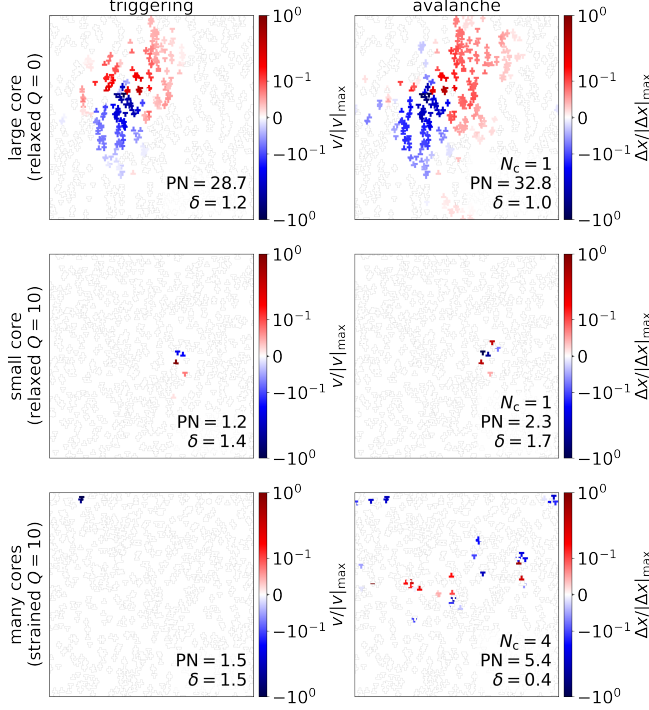


FIG. 9. Left: The dislocation velocity v at the triggering at three typical events. Right: The displacement Δx accumulated during the same events. The participation number PN (based on either the velocities or the accumulated displacements), the exponent δ characterizing the decay of either $\langle v_i v_j \rangle$ or $\langle \Delta x_i \Delta x_j \rangle$ at large distances and the number of avalanche cores N_c are also shown for each event. For the definition of these quantities see the main text. Note: the point defects are not indicated in the figure for visibility purposes.

The visual inspection of the avalanches revealed that the events can be categorized into three classes that are presented in Fig. 9. Some events are already quite extended at their onset and naturally the accumulated plastic activity also covers a large portion of the simulation cell (see top row of Fig 9). Other events are triggered very locally and remain small during the avalanche (see middle row). The probably most interesting type of event is the third one where the triggering occurs locally and then small clusters of dislocations (or even single dislocations) are drawn into motion from remote regions of the sample (see bottom row). That is, instead of the growing of a single core of active dislocations a ‘sea-islands’ type picture emerges.

In order to statistically quantify the differences of events in the four scenarios a simple algorithm is introduced to detect clusters of active dislocations and classify plastic events into the three casts presented in Fig. 9. To this end, the accumulated dislocation activity during the avalanches is considered. First, all dislocations with a total displacement below 1% of the largest individual dislocation displacement are discarded and only the ones

with displacements above this threshold are kept. Then all dislocation that are within the distance of $3d$ (where $d = L/\sqrt{N}$ is the average dislocation spacing) are virtually connected. The connected clusters of dislocations are considered the cores of the avalanche. Finally, the number of clusters consisting of more dislocations than the third of the size of the largest core are counted and is denoted by N_c (for examples see Fig. 9). Additionally, $PN(\Delta x)$ is computed (including all N dislocations). The classes are then determined as follows. If $N_c > 2$, the event is categorized to have ‘many cores’. If not, that is if it only has 1 or 2 cores, and $PN(\Delta x) > N/100 = 10.24$ then the event is classified as having a ‘large core’, otherwise, it has a ‘small core’. We note that while the choice of thresholds for the number of cores and for the participation number is arbitrary, the same conclusions can be drawn within a sensibly wide range of thresholds.

The execution of this classification on the four scenarios reveals the following picture that is visualized in Fig. 11. As it was shown, the behavior of relaxed $Q = 0$ and $Q = 10$ systems (scenario I and II) is fundamentally different. In $Q = 10$ configurations practically all plastic events are quite small while in the $Q = 0$ samples there is a wide selection of events ranging from the motion of single dipoles ($PN \approx 2$) up to events well above our threshold of $N/100 = 10.24$ (see also Fig. 8). It is the same, however, in both cases that the core of the avalanche is typically one spatially compact active region. The picture is more complex as the $Q = 10$ configuration is strained and approaches the phase transition to the state of sustained flow (scenario III). While the growth in terms of PN is incremental, the activation of many small and spatially disjoint parts of the sample during the avalanche is significantly (c. four times) more frequent than in the relaxed case. Individual dislocation velocity data suggests that remote dislocation clusters are drawn into the avalanche by subsequent chain-triggering (see Fig. 10 for an example). This explains the conundrum how the long-range dynamical correlations appear in the strained systems even though the size of the avalanches (in terms of the number of participating dislocations) does not increase proportionally at all. It can be also observed that upon unloading $Q = 10$ systems (scenario IV) return to the same behavior characterizing their relaxed counterparts (scenario II) despite their pre-deformation history.

It was demonstrated in previous works that at small strains pure (point defect free) dislocation systems (scenario I) and the ones also containing a great extent of short-range quenched disorder (in the form of, e.g., point defects or precipitates, scenario II) belong to two distinct classes [21, 29]. This has been observed here as well: in both scenarios I and II the avalanches have a single compact core, however, while in scenario I localized and extended events coexists, in scenario II practically all avalanches are localized. The current results imply that the avalanche behavior of immensely strained systems with quenched disorder (scenario III) belong to a

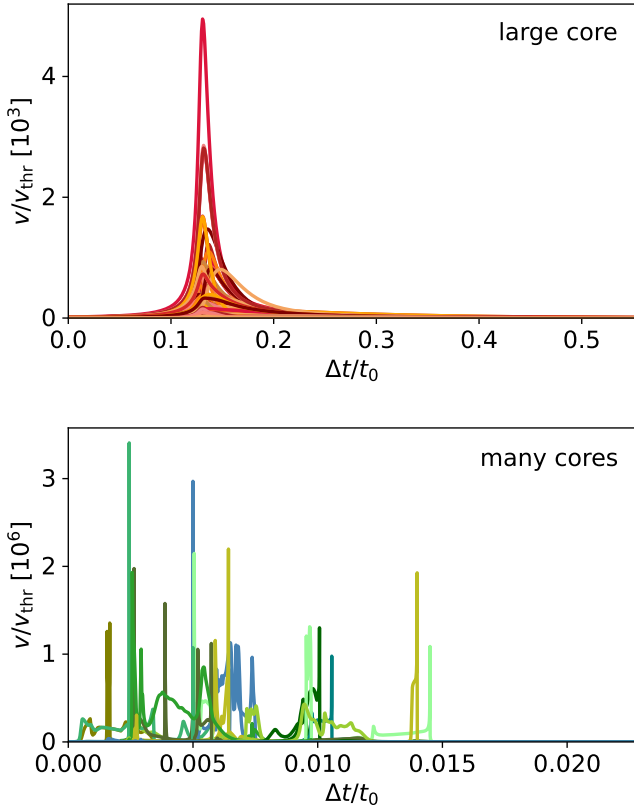


FIG. 10. Comparison of the dislocation velocity evolution during avalanches for the two types (single-core and multi-core) of spatially extended plastic events. Each curve denotes the magnitude of the velocity v (normalized with the avalanche detection threshold v_{thr}) of an individual dislocation. Time Δt starts at the onset of the avalanche and is measured in simulation unit t_0 . (Top): A typical single-core event (corresponding to the ‘large core’ example in Fig. 9) which has a relatively smooth and uniform velocity evolution. (Bottom): A typical multi-core avalanche (corresponding to the ‘many cores’ example in Fig. 9) characterized by the chain-triggering of remote dislocations (or clusters of dislocations) resulting in an intermittency of the evolution of dislocation velocity.

third, different regime. In these systems there is diversity of events affecting very local and very extended regions of the sample, but even in the latter case the avalanches consist of a small number of dislocations which are, however, from clusters scattered along the specimen. The proposed phase diagram supplemented with the new regime is schematically shown in Fig. 12 with caption briefly summarizing the nature of avalanches in each regime. It should be stressed that the figure is strictly schematic and the actual shapes of different regimes can not be obtained from the current data.

	$Q = 0$	$Q = 10$		
large core	51	0	1	0
many cores	0	3	11	3
small core	49	97	88	97
	relaxed I	relaxed II	strained III	prestrained IV

FIG. 11. The classification of the first avalanches of the 100 configurations of each type. Relaxed $Q = 0$ systems exhibit a diversity between of small and large typically single-core avalanches. Relaxed and prestrained $Q = 10$ configurations almost exclusively produce small single-core avalanches while a significant minority of multi-core but typically relatively low-PN events emerges in strained systems. For the details of the classification method and the definition of the three classes see the main text.

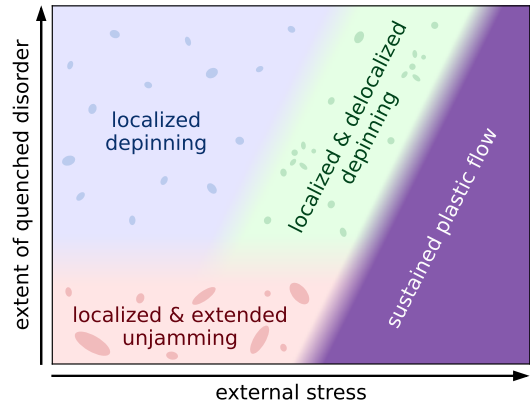


FIG. 12. The regimes of dynamic behavior during avalanche activity. At low external stress in systems dominated by long-range dislocation-dislocation interactions avalanches occur due to the unjamming of dislocations in form of compact events that come from a very wide size-range. At low external stress in systems dominated by short-range interactions upon depinning small localized avalanches occur. At larger stresses however, a significant minority of delocalized avalanches appear which consist of small clusters of moving dislocation scattered across a large area. At large enough stress (which is dependent on the extent of short-ranged quenched disorder) the system reaches the state of sustained plastic flow.

E. Yield stresses and local yield stresses

After studying the correlations and the avalanche behavior now we turn to one of the main questions if this work: how are the local yield stresses affected by the

avalanches and the deformation of the model sample. Firstly, the long-term, global impact of the deformation is studied. That is, the effect of severely straining and then unloading the system on the statistics on the yield stresses. Then, the short-term, local impact is investigated. Namely, how the local yield stress landscape evolves due to individual avalanches in the four different scenarios.

The local yield stress associated with a given sub-region of the sample (referred to as *box* in the rest of the paper) is assumed to be determined by the strength of the weakest of the activable substructures (links) within the box. (If the local yield stress is assigned to the whole simulation cell, we will simply refer to it as the yield stress or yield threshold). Thus, one may expect the local yield stress τ_y to obey an extremal probability distribution, in particular, a first order statistics (i.e., minimum) distribution. Namely, if in the small strength limit the link strength τ_{link} is powerlaw distributed as $F_{\text{link}}(\tau_{\text{link}}) \propto \tau_{\text{link}}^k$, F_{link} being the cumulative distribution function (CDF) of τ_{link} , then the emergent extremal distribution is of Weibull type [30–34] with a CDF

$$F(\tau_y) = 1 - \exp \left[- \left(\frac{\tau_y}{\lambda} \right)^k \right]. \quad (11)$$

Here λ and k are the so-called *scale* and *shape parameters*, respectively. The former is proportional to the mean value of the variable and the latter describes the asymptotic behavior at the $\tau_y \rightarrow 0$ limit. Here we consider $\tau'_y = \tau_y - \tau_{\text{init}}$ where τ_{init} is the initial external stress which is zero for all scenarios except scenario III. The statistics of yield thresholds τ'_y (corresponding to the whole simulation cell) were obtained during loading the sample with a quasi-statically increasing spatially homogeneous external stress, τ_y being the critical stress at which the first avalanche occurs. The event is detected based on thresholding: the avalanche is considered to have started when both the mean dislocation velocity and its derivative w.r.t time exceed a predefined value. As it is shown in Fig. 13 the statistics of the yield thresholds τ'_y indeed obeys the Weibull distribution with a shape parameter $k \approx 1.1 \pm 0.1$ robust to the change of the extent Q of quenched disorder and to the deformation history of the sample. The scale parameter λ , however, depends on Q and the deformation history. The most significant effect is that prestraining (scenario IV) immensely increases the yield stress values due to the elimination of weak substructures that are easy to trigger during the loading stage.

Above it was shown that while some features (e.g. the shape parameter) of the yield threshold distribution is robust, the straining history can affect the statistics of local yield stresses. Now let us focus on the short-term changes of local yield stresses (corresponding to smaller subsystems) after individual dislocation avalanches. To this end the following procedure is applied. Each configuration is divided into 8×8 square shaped disjoint boxes. Then the local yield stress of each box is probed

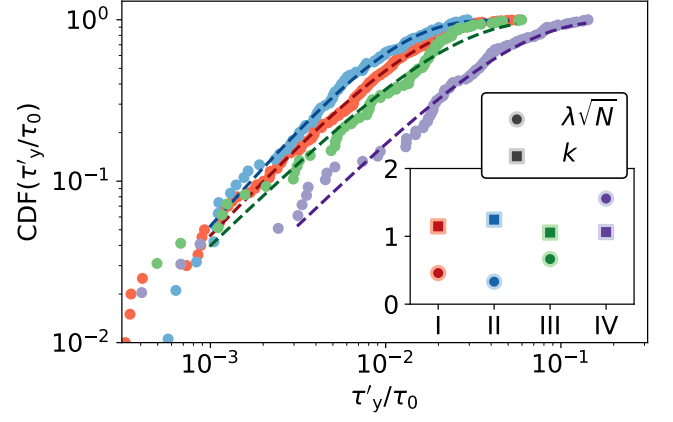


FIG. 13. The cumulative distribution functions (CDFs) of the corrected yield stress $\tau'_y = \tau_y - \tau_{\text{init}}$ where τ_y and τ_{init} are the yield stress and the initial external stress, respectively. The latter is non-zero only in the strained (green) case. The inset shows the scale (k) and shape (λ) parameters of the fitted Weibull distributions. τ_0 is a constant defined in the main text and $N = 1024$ is the number of dislocations.

by quasi-statically increasing spatially homogeneous external stress while keeping the dislocations outside the box fixed. The computation of local yield stresses is done with the thresholding-based detection of avalanches described above. The local yield stresses are first computed for all boxes based on the first avalanches. Then, quasi-static global loading is applied to the relaxed configurations. That is, all dislocations are affected by the homogeneous external stress and all are mobile. The configurations are loaded until the first avalanche occurs (that is, until the yield threshold of the whole simulation cell). This, naturally results in the spatial redistribution of dislocations which leads to the change of the local yield stress of each fictitious box. The local yield stresses are measured after this global loading as well. The change of τ_y is denoted with $\Delta\tau_y$. For each configuration a map of $\Delta\tau_y$ is created. The box with the largest change (in terms of absolute value) is considered to be the core of the avalanche was. Each map is rearranged by moving the core box into the center while keeping the relative positions (quantified by coordinates Δx and Δy) of boxes (taking into account the PBC). These re-centered maps are then averaged (and symmetrized in order to decrease noise) over the ensembles of configurations of each of the four scenarios. The so obtained maps of $|\Delta\tau_y|$ and $\Delta\tau_y$ are shown in Figs. 14 and 15, respectively.

The maps indicate that at the core box (that is, where the dislocation avalanche emerged) $\langle |\Delta\tau_y| \rangle$ is significantly larger than in any other box and $\langle \Delta\tau_y \rangle > 0$, that is, an immense hardening is observed. This is not surprising since after the activation of the first avalanche the next activable link is probably significantly harder to trigger. This can be explained by the assumption (consistent with the numerically obtained Weibull distributions of τ_y) that the low-strength asymptotic distri-

bution of link strengths obeys a power-law. This is the part of the distribution that matters during weakest link activation. Since at the low-strength tail of the distribution the probability density is low, independently of the redistribution of dislocations, one's intuition would be that the second avalanche in this core box is significantly harder to trigger than the first one. The other boxes are also affected by the avalanche but to a smaller extent and typically softening can be observed instead of hardening. The probability density functions of $\Delta\tau_y$ are shown in Fig. 16. The core boxes almost always (with more than 93% probability in each scenario) harden with $\Delta\tau_y$ approximately obeying an exponential distribution. The non-core boxes typically soften (with more than 76% probability in each scenario) due to the increased external stress and the change of internal stresses resulted by the dislocation rearrangements.

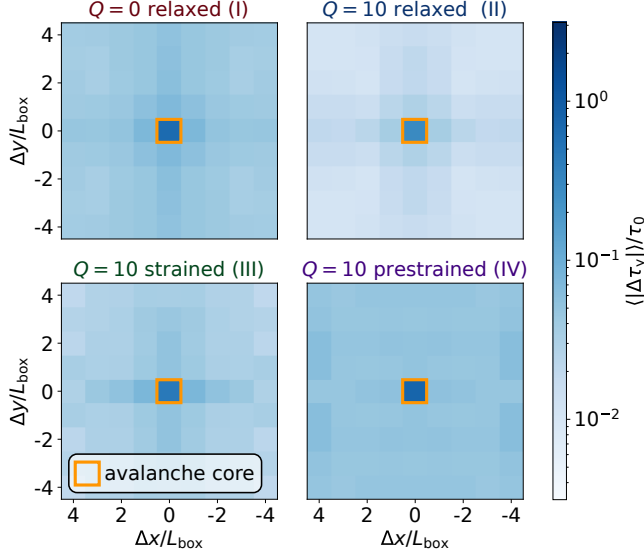


FIG. 14. The average of the absolute value of the change of the local yield stresses $\langle |\Delta\tau_y| \rangle$ in the boxes. Δx and Δy are the relative coordinates measured from the middle of the box where $|\Delta\tau_y|$ is the largest. L_{box} is the edge width of the boxes and τ_0 is a constant defined in the main text.

Figure 17 shows the dependence of $\langle |\Delta\tau_y| \rangle$ on the distance $\Delta r = \sqrt{\Delta x^2 + \Delta y^2}$ measured from the avalanche core. In every scenario the impact of the avalanche on the local yield stresses decay according to

$$\langle |\Delta\tau_y| \rangle \propto (\Delta r)^{-\beta}. \quad (12)$$

As in relaxed $Q = 10$ systems (scenario II) the dynamical correlations are weaker and shorter-ranged than in their $Q = 0$ counterparts (scenario I), not surprisingly, the same can be observed in terms of the magnitude of $\langle |\Delta\tau_y| \rangle$ and the exponent β . More surprisingly, β remain the same during severe straining (scenario III), although, the avalanche impact is stronger (comparable with scenario I) indicated by the increase in the magnitude of $\langle |\Delta\tau_y| \rangle$. In the pretraining case (scenario IV) $\beta \approx 0$,

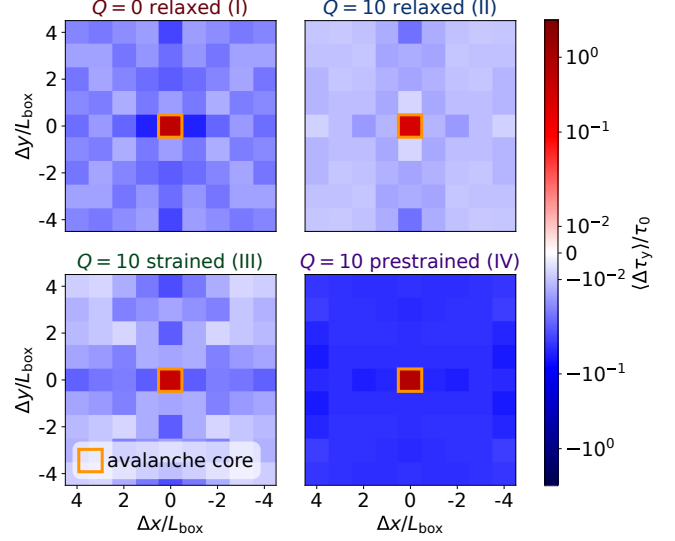


FIG. 15. The average of the change of the local yield stresses $\langle \Delta\tau_y \rangle$ in the boxes. Δx and Δy are the relative coordinates measured from the middle of the box where $|\Delta\tau_y|$ is the largest. L_{box} is the edge width of the boxes and τ_0 is a constant defined in the main text. The middle box (where the avalanche core is) exhibits a significant hardening while the surrounding boxes show softening on average.

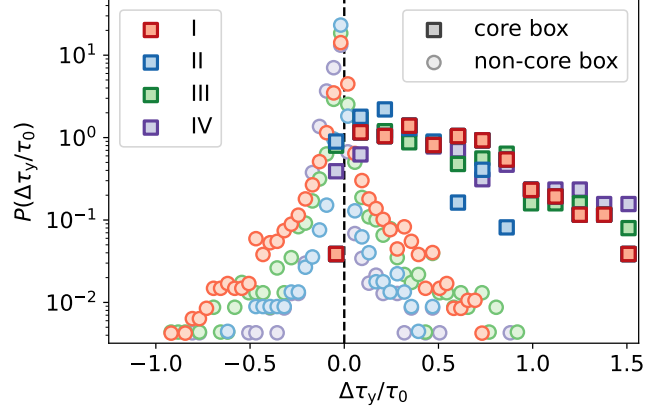


FIG. 16. The probability density function P of the change of local yield stresses $\Delta\tau_y$ in core boxes (where the core of the avalanche is) and non-core boxes. The core boxes almost always exhibit strong hardening and the non-core ones typically show weak softening. τ_0 is a constant defined in the main text and the dashed line underscores $\Delta\tau_y = 0$.

that is, the softening is comparable in all boxes. This is the results of the first avalanche being triggered after an increment of external stress much larger than in any other scenarios which leads to a larger extent of rearrangement (in the form of drifting dislocation motion) prior to the avalanche. This is probably related to the elimination of substructures that are easy to trigger during the pretraining (which was also suggested in Ref. [35]).

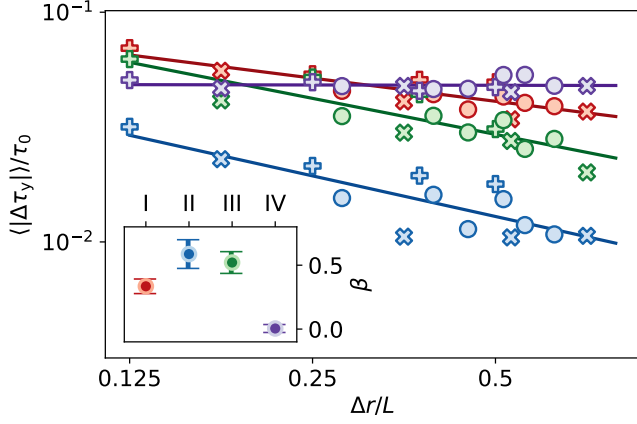


FIG. 17. The average of the absolute value of the change of the local yield stresses $\langle |\Delta\tau_y| \rangle$ in the boxes as a function of the distance Δr of their middle from the middle of the box that contains the core of the avalanche (that is, where $|\Delta\tau_y|$ is maximal). ‘+’: box horizontally or vertically aligned with the core box, ‘x’: box diagonally positioned in comparison to the core box, ‘o’: every other box. The inset shows the exponent β characterizing the powerlaw decay with the distance from the core box. L and τ_0 are the linear size of the simulation cell and a constant defined in the main text, respectively.

It is generally true (regardless of the scenario) that the boxes that are vertically or horizontally aligned with the core box are more impacted by the avalanche while the diagonally positioned boxes are less affected. This angular dependence can be related to the stress field induced by the rearrangement of the dislocations by the inspection of the Eshelby stress field of a displaced dislocation [36]. The shear stress field of a dislocation displaced with an infinitesimally small Δx changes with $\Delta\tau = \partial_x \tau_d \Delta x = \frac{\cos(4\varphi)}{r^2} \Delta x$ where φ is the angular polar coordinate and τ_d is the shear stress field of a dislocation (see Eq. (1)). If it is assumed that (i) during an avalanche the displacement of dislocations is typically small, (ii) most of the dislocations move in the direction consistent with the external stress and (iii) the dislocation motion is the most intense in a relatively local and compact inner core of the avalanche, the change of the internal stress field has roughly a $\cos(4\varphi)$ type angular dependence (consistently with the results in Ref. [29]) which strengthens the effect of the external stress in the vertical and horizontal directions and weakens it diagonally. This leads to the observed enhanced softening vertically and horizontally and the mitigated softening diagonally.

IV. CONCLUSION AND OUTLOOK

In this work we studied the static and dynamic length scales, avalanche dynamics and local yield stresses in 2D DDD framework in configurations with and without

short-range quenched disorder and with different deformation history. As the pure systems driven exclusively by long-range elastic interactions exhibit criticality already at zero external stress, our focus was on whether and how the behavior of systems with quenched disorder (dominated by short-range interactions) tend to the criticality characterizing the pure systems. Therefore, while using the relaxed systems (with or without short-ranged quenched disorder) as references we examined the behavior of systems with quenched disorder after severely straining (loading) them and also after subsequent unloading.

In terms of static dislocation-dislocation correlations it was found that the straining, despite making the correlation weaker, also makes it longer-range which effect persisted after unloading the sample as well. Similarly, the severely strained systems (despite avalanches being triggered very locally, in contrary to pure systems) exhibited longer-range dynamic correlations than their relaxed counterparts (unlike the unloaded/prestrained configurations). However, further analysis of the data revealed that this avalanche behavior, despite exhibiting similar asymptotic dynamic correlations compared to pure systems, fundamentally differs from the nature of plastic events in the systems dominated by long-range interactions. Our results imply that apart from the regime of sustained plastic flow at very large stresses at least three distinct regimes of avalanche behavior exist in this framework. Namely, (1) when long-range dislocation-dislocation interaction dominate the dynamics, localized and extended plastic events coexist and they occur as a result of dislocation unjamming. In systems dominated by short-range interactions (2) at low external stress plastic events are localized and happen due to depinning of dislocations, however, (3) at larger stresses, in addition to localized events, another type of avalanche appears. These events are typically also triggered locally but the triggering is followed by a delocalized sequence of depinning of small, spatially isolated and often quite remote clusters of dislocations. That is, while in this regime the extended dynamic correlations indeed appear similarly to the pure systems these correlations are not the result of the correlated motion of a large and compact dislocation cluster but the chain-triggering of a lower number of dislocations scattered across a quite extended region of the system.

Besides the correlations, the yield stress (corresponding to whole configurations) and local yield stresses (corresponding to subsystems) were studied. The results showed that the yield stresses (consistently with the weakest-link principle) obey Weibull distribution with a shape parameter robust to the introduction of quenched disorder and to the deformation history. It was observable, however, that the loading and subsequent unloading of a configuration results in a remarkable hardening (that is, a shift of the scale parameter of the yield stress distribution). The analysis of local yield stresses indicate that the local hardness of the material changes significantly

when an avalanche occurs due to the rearrangement of dislocations. At the core of the avalanche an immense hardening is observable. In the more remote vicinity, however, the material is (on average) softening and the impact is significantly weaker. The softening effect diminishes as the distance from the core of the avalanche is increased. More precisely, the mean change of the local yield stress decays according to powerlaw with an exponent dependent on the extent of quenched disorder and the straining history and it exhibits an angular dependence consistent with the Eshelby stress field.

We note that our results were performed in a relatively simple 2D DDD model which as such can reproduce statistical features of crystalline plasticity in single-slip

setup (such as in appropriately oriented HCP materials) but it cannot account for more complex behavior prevalent in multi-slip scenarios, e.g., junctions, cross-slip, etc. It still remains to be challenging, however, to study the high-strain regime for sufficiently large samples in the 3D DDD framework due to the immense computational cost. This computational barrier and the easier interpretability of the 2D model led us to employing 2D DDD for this particular study. Nevertheless, it would be an interesting question in the future to see how severe straining affects the static and dynamic correlations and local yield stresses in more complex 3D DDD models and whether a similar picture emerges in terms of the prevalent regimes of avalanche behavior.

-
- [1] N. Fleck, G. Muller, M. Ashby, and J. Hutchinson, *Acta Metallurgica et materialia* **42**, 475 (1994).
 - [2] M. D. Uchic, D. M. Dimiduk, J. N. Florando, and W. D. Nix, *Science* **305**, 986 (2004).
 - [3] M. D. Uchic, P. A. Shade, and D. M. Dimiduk, *Annual Review of Materials Research* **39**, 361 (2009).
 - [4] D. M. Dimiduk, C. Woodward, R. LeSar, and M. D. Uchic, *Science* **312**, 1188 (2006).
 - [5] F. F. Csikor, C. Motz, D. Weygand, M. Zaiser, and S. Zapperi, *Science* **318**, 251 (2007).
 - [6] J. Weiss and J.-R. Grasso, *The Journal of Physical Chemistry B* **101**, 6113 (1997).
 - [7] J. Weiss and D. Marsan, *Science* **299**, 89 (2003).
 - [8] J. Weiss, W. B. Rhouma, T. Richeton, S. Dechanel, F. Louchet, and L. Truskinovsky, *Physical review letters* **114**, 105504 (2015).
 - [9] P. D. Ispánovity, D. Ugi, G. Péterffy, M. Knapek, S. Kalácska, D. Tüzes, Z. Dankházi, K. Máthis, F. Chmelík, and I. Groma, *Nature communications* **13**, 1975 (2022).
 - [10] F. Spaepen, *Acta metallurgica* **25**, 407 (1977).
 - [11] M. L. Falk and J. S. Langer, *Physical Review E* **57**, 7192 (1998).
 - [12] A. Kabla and G. Debrégeas, *Physical review letters* **90**, 258303 (2003).
 - [13] M. Dennin, *Physical Review E* **70**, 041406 (2004).
 - [14] O. Tainio, L. Viitanen, J. R. Mac Intyre, M. Aydin, J. Koivisto, A. Puisto, and M. Alava, *Physical Review Materials* **5**, 075601 (2021).
 - [15] D. Richard, M. Ozawa, S. Patinet, E. Stanifer, B. Shang, S. Ridout, B. Xu, G. Zhang, P. Morse, J.-L. Barrat, *et al.*, *Physical Review Materials* **4**, 113609 (2020).
 - [16] S. Patinet, D. Vandembroucq, and M. L. Falk, *Physical review letters* **117**, 045501 (2016).
 - [17] D. Berta, G. Péterffy, and P. D. Ispánovity, *Physical Review Materials* **7**, 013604 (2023).
 - [18] A. Barbot, M. Lerbinger, A. Hernandez-Garcia, R. García-García, M. L. Falk, D. Vandembroucq, and S. Patinet, *Physical Review E* **97**, 033001 (2018).
 - [19] J. R. Morris, H. Bei, G. M. Pharr, and E. P. George, *Physical review letters* **106**, 165502 (2011).
 - [20] C. Liu and R. Maaß, *Advanced Functional Materials* **28**, 1800388 (2018).
 - [21] M. Ovaska, L. Laurson, and M. J. Alava, *Scientific reports* **5**, 1 (2015).
 - [22] X. Pan, W. Hu, and C. Wu, *Journal of the Mechanics and Physics of Solids* **103**, 3 (2017).
 - [23] D. Berta, I. Groma, and P. D. Ispánovity, *Modelling and Simulation in Materials Science and Engineering* **28**, 035014 (2020).
 - [24] H. Shima, T. Sumigawa, and Y. Umeno, *Materials* **15**, 4929 (2022).
 - [25] G. Péterffy and P. D. Ispánovity, *Modelling and Simulation in Materials Science and Engineering* **28**, 035013 (2020).
 - [26] M. Zaiser, M.-C. Miguel, and I. Groma, *Physical Review B* **64**, 224102 (2001).
 - [27] I. Groma, G. Györgyi, and B. Kocsis, *Physical review letters* **96**, 165503 (2006).
 - [28] P. Derlet and R. Maaß, *Physical Review E* **94**, 033001 (2016).
 - [29] P. D. Ispánovity, L. Laurson, M. Zaiser, I. Groma, S. Zapperi, and M. J. Alava, *Physical review letters* **112**, 235501 (2014).
 - [30] W. Weibull, *IVB-Handl.* (1939).
 - [31] W. Weibull, *Journal of applied mechanics* **103**, 293 (1951).
 - [32] P. M. Derlet and R. Maass, *Philosophical Magazine* **95**, 1829 (2015).
 - [33] P. Derlet and R. Maaß, *Scripta Materialia* **109**, 19 (2015).
 - [34] P. D. Ispánovity, D. Tüzes, P. Szabó, M. Zaiser, and I. Groma, *Physical Review B* **95**, 054108 (2017).
 - [35] H. Salmenjoki, M. J. Alava, and L. Laurson, *Nature communications* **9**, 5307 (2018).
 - [36] J. D. Eshelby, *Proceedings of the royal society of London. Series A. Mathematical and physical sciences* **241**, 376 (1957).